Uncovering Modular Structure Underlying Gated Information Transfer in the Mouse Premotor Cortex

Mika Jain, Jack Lindsey, and Jiren Zhu
Stanford University
lindsey6,mjain4,jirenz@stanford.edu

Abstract

We develop, validate, and apply network analysis tools to neural recordings from mice, uncovering structural features of neuronal networks in premotor cortex (ALM) in the left and right hemispheres of the mouse brain. We infer neuronal network structure using measures of activity correlation, causality, and behavioral prediction similarity between pairs of neurons. Next, we validate these methods using simulations with known ground-truth connectivity patterns. We compute summary statistics over the inferred network structure that indicate substantial cross-hemisphere communication. We apply a variety of community detection algorithms uncover modular structure, finding that it spans across anatomical regions and demonstrate and is robust to experimental optogenetic perturbation of ALM. Further more, we find that certain measures of modularity in the inferred networks are predictive of behavioral and neural activity differences across mice.

1. Introduction

Modern experimental techniques allow for large-scale recording and perturbation of neural activity at neuron resolution. Existing work has shown that mice can perform motor tasks correctly when left or right (but not both) ALM is perturbed optogenetically by experimenters [4]. This work suggests that there exists a correction and information recovery mechanism between the left and right premotor cortex (ALM). While experimental techniques allow for separate analysis and perturbation of distinct anatomical regions like left and right ALM, they do not allow for

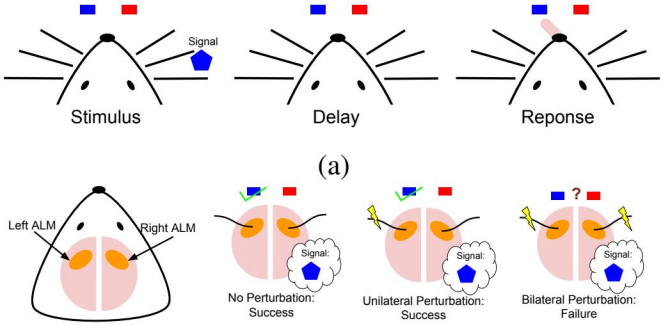

Figure 1. (a): Mice are trained to lick in one of two directions after receiving a stimulation. (b): Optogenetic perturbation is applied to left and/or right ALM region during the delay period. When no peturbation is present or only one side is perturbed, mice can still perform the task properly. When both ALMs are perturbed, mice cannot perform the task any more.

Code for this project publicly available at https://github.com/jlindsey15/224WProject

Contributions: Mika: net. denoising, panel of comm. detect. algs., signif. testing, graph & community visualizations. Jiren: net. construction, edge weight / node degree metrics, simulation, L/R modularity analysis. Jack: preprocessing, net. construction, edge/node metrics, validated spectral clust. across sessions, L/R mod. analysis

direct examination of underlying modular neural structures that may exist at a finer scale, or which may in fact span multiple regions. Since neurons are known to interact in complex networks, applying network analysis algorithms to time-series neural data has the potential to uncover modular structures and interactions between them at the appropriate scale and level of abstraction. We seek to uncover structure that lies within and across anatomical hemispheres and use variability in these structures across mice and experimental sessions to predict behavioral differences in task performance.

2. Related Work

Gated information transfer in mice premotor cortex. The work of [4] demonstrated modular structure in left and right mouse premotor cortex (ALM). Mice were trained on a task which required them to choose one of two motor outputs according to a sensory stimulus. A delay period was imposed between the stimulus in response. See Figure 1. Electrode-array recordings of neural activity in left and right ALM during the delay period are predictive of mouse motor output (left or right). Bilateral optogenetic silencing of left and right ALM simultaneously during the delay period prevent the mouse from performing the task correctly. After such a perturbation, ALM activity immediately before the motor response is still predictive of the response, but diverges significantly from its average values on control trials. However, following a unilateral silencing of left or right ALM, the mouse can still perform the task correctly, and the silenced hemisphere recovers its typical activity. See Figure 1. These results indicate that there is modular structure in the ALM system, as the damage to the information in the perturbed ALM does not propagate to the unperturbed side. However, there must be information transfer between left and right ALM, in the direction of the perturbed side, since the activity on the perturbed side recovered. [4] showed that these results could not be accounted for well by a linear model of the entire left/right ALM system but could be explained by considering left and right ALM as modules with gated, nonlinear interaction.

Correlation-based functional networks. One common technique to infer functional connectivity structure from neural data is assigning undirected network edge strengths according to the strength of correlation in firing rate activity between pairs of neurons. This approach has allowed previous work to identify interesting network structure underlying neural activity – for instance, [8] found small world structures in brain functional networks. However, this technique has been shown to sometimes overestimate network clustering ([11]), and care is required in null model construction to avoid identifying spurious network structures.

Granger causality-based functional networks. Instead of using correlation, one can employ metrics that capture causal relationships between the time-series activity of neurons. Some examples are transfer entropy [9] and Granger causality [3]. These techniques quantify the causal influence of A on B by measuring the additional information that the present value of A provides about B's future beyond what B already provides. These methods yield *directed* graphs and widely used for discovering interactions between neurons and brain regions. For instance, [5] constructed causality-based functional networks from multi-subject EEG measurements and performed community detection using an adapted version of the Louvian algorithm. [6] identified communities of well connected "rich-club" neurons using a causality-based network derived from electrode-measured neuron activities.

Community detection. A number of community detection algorithms can be used to infer modular structure in functional networks. The

Clauset-Newman-Moore algorithm [1] greedily maximizes network modularity by first assigning each node to its own community and then joining pairs of communities that increase modularity until no such pair exists. Label propogation [10] first assigns each node its own community label and then repeatedly change the label of each node to the most frequent label of it neighbors until no further changes can be made. Communities discovered with label propagation depend significantly on if label updates are performed in parallel on all nodes (synchronous model) or sequentially (asynchronous model). [2] introduces a hybrid, semi-synchronous model that is more stable than asynchronous models and as fast as synchronous models. The fluid community algorithm [7] is inspired by label propagation models. The algorithm first randomly initializes each of k community labels to a unique node and then iterates over each node, setting its label to the community with maximum density within the ego network of the node. Density is calculated as the reciprocal of the number of vertices in a community.

3. Methods

3.1. Data and Preprocessing

Dataset. This data is available courtesy of Prof. Shaul Druckmann (Neurobiology) and Prof. Nuo Li (Baylor College of Medicine). Mice are trained to perform the following task: first, the mice are stimulated with a pole in one of two locations in their whiskers. Next a "delay period" is imposed, followed by an auditory "go" cue. After the cue, the mice respond by licking one of two ports, according to which of the two stimuli they perceived – the responses we refer to as "lick left" and "lick right." Silicon probes are used to record spiking activity of populations neurons in left and right ALM throughout the performance of the task. On some trials, optogenetic perturbation is used to silence neural activity on one (unilateral – left ALM or right ALM) or both (bilateral) ALM regions during the delay period.

The coding direction referred to in subsequent analysis is computed as the difference in average activity for lick-right trials and the average activity for lick-left trials in the last time bin of the delay period on control (no stimulation) trials. The coding direction is, essentially, the linear combination of population activity that provides the most predictive information about the mouse's response before the response occurs.

Preprocessing The raw spiking neural data requires careful preprocessing to produce meaningful time-series firing rate data. Ultimately, the preprocessed data consists of time-series estimates of the real-valued firing rates of each neuron in the recording, throughout the experimental delay period. See the Appendix for details.

3.2. Inferring network structure.

As described above, the dataset contains time-series observations of firing rates of populations of neurons. Each neuron is treated as a node. We employ several methods to infer edge weights between nodes, for both control trials and bilateral perturbation trials. They are described below. Network structures are inferred independently for each experimental session.

Activity Correlation. First, we infer functional undirected connectivity sturcture between neurons, assigning edge weights equal to the absolute value of the Pearson correlation of activity of each pair of neurons.

Granger Causality. Second, we infer functional directed connectivity structure, assigning directed edge weights as follows. For each pair (A, B) of neurons, we fit the best linear regressor that predicts B_{t+1} from B_t across all trials and time steps in the dataset, where time steps are of length 0.1 s. Then a linear regressor is fit that predicts the residual error of the first regressor from A_t. The significance (p-value) of this last prediction, as determined by a t-test, is used to assign

directed edge weights – specifically, edge weights are set to $1 - p$.

Behavioral Prediction Similarity. Neural activity in left and right ALM during the delay period is predictive of mouse behavior (lick-left vs. lick-right). This is even the case on trials in which the mouse performs the task incorrectly (i.e. when the mouse does not give the response that corresponds to the stimulus). The best linear predictor of behavior (fit via logistic regression) using neural activity immediately before the go cue has 94 % accuracy on control trials and 89 % accuracy on bilateral perturbation trials. The predictivity is not perfect – individual neurons, in particular, make inaccurate predictions on many trials. We leverage these effects to produce another measure of similarity between neurons – the frequency with which neurons make the same behavioral prediction (normalized to lie in [0, 1] where 50% agreement corresponds to 0 and 100% agreement corresponds to 1). The predictor for each neuron is obtained by fitting a logistic regression model to predict behavioral output (lick-left vs. lick-right) from that neuron's firing rate activity immediately before the go cue, across trials.

Validating our Network Construction Methods. To validate and characterize the limitations of our network construction methods, we perform a simulation study. We construct a model of neuron connectivity and firing behavior and assess how well our edge weight inference methods are able to infer the ground truth connectivity. We were particularly interested in the following questions.

1. How well do the correlation cetwork and the causality network capture true relations between neurons?

2. Is the causality network capable of capturing asymmetric relations?

We simulate neural activity firing using the following model. Neurons are connected in a directed fashion. All result are evaluated over N trials. In each trial, there are T time steps. For each $t \in \{1, 2, ..., T\}$, there are W opportunities for a neuron to fire. There are three conditions that control the probability with which a neuron fires. 1) A neuron A fires at time (t, w) with intrinsic probability p. 2) If A fired at time $(t-1, w)$, then with probability r it will fire at (t, w). 3) If all parents of A fired at time $(t-1, w)$, then with probability q A will fire at (t, w). $f(A, t, w) = 1$ if A fired at time t, w, 0 otherwise. At time step t, the observed firing rate for neuron A, $v(A, t)$, is the sum over all w firing opportunities. $v(A, t) = \sum_{w=1}^{W} f(A, t, w)$. The construction is designed to have several properties. It is straightforward to see that if B has sole parent A,

$$E[v(B,t)] = p + rE[v(B,t-1)] + qE[v(A,t-1)].$$

For each neuron, firing rate at time t has autocorrelation with firing rate at $t-1$ (controlled by r). Additionally, there can be causal relationship between neuron firing rates (controlled by q).

We base our simulation parameters on the control (no-perturbation) experimental condition. Unless otherwise specified, each session contains $N = 100$ trials. Each trial records $T = 15$ time steps. $p = q = r = 0.3$. In the most simple case, the connection is $A \to B$, C connected to nothing. Two examples of firing rate time series can be seen in Figure 2 (a) & (b). Under our construction, A has causal correlation to B but the time series are very noisy, which is representative of what would happen with real life data.

We varied the true interaction strengths q and the number of observed trials N and characterized the ability of our correlation metric and Granger causality metric to uncover true relationships between neurons.

3.3. Community detection.

We sought to uncover community structure in the inferred networks. Our goal was to discover

whether (1) Community structure persists even in the face of perturbation, and (2) Which control trial graph construction method is best suited to predicting community structure following perturbation. Community detection involves a number of modeling choices, including the choice of community detection algorithm and the method of preprocessing. Given the level of noise in our data, no method is guaranteed to uncover important structure even if it exists, so using a diverse array of methods is important. In particular, we found that applying a panel of community detection methods to pruned, unweighted graphs on a representative experimental session was helpful in allowing us to clearly establish and visualize persistence of community structure in the various graph types before and after perturbation. Next, we focused on the case of applying spectral clustering to the original weighted graphs in order to quantify more thoroughly the extent to which structure in the control trial graphs predicted community structure in graphs with different constructions and in bilateral perturbation graphs.

Panel of Community Detection Algorithms. We use a panel of six algorithms to detect community structures. The panel consists of the Clauset-Newman-Moore algorithm (greedy modularity), asynchronous label propagation, semi-synchronous label propagation, spectral clustering, and Kernighan-Lin algorithm (all discussed above). Each functional network is constructed from activity data during either baseline state or bilateral perturbation, and has edge weights deriving from either activity correlation, Granger causality, or behavioral predication similarity.

Networks were denoised prior to community detection by keeping only edges with weights within the the P-th percentile. Community detection was found to depend significantly on P, which was varied during each experiment. To further reduce noise, we only consider communities with more than two nodes and fewer than 80% of the total number of nodes in each network.

The communities of greatest interest correspond to modular network structure that is invariant to perturbation, i.e. communities that are observed both in networks constructed from baseline activity and from activity during bilateral perturbation (importantly, the neurons being recorded are the same). We take the similarity of two clusters from different networks to be $J(V_1, V_2)$ where V_1 and V_2 are the vertices in each cluster and J is the Jaccard index defined as

$$J(V_1, V_2) = \frac{|V_1 \cap V_2|}{|V_1 \cup V_2|}.$$

We report the significance of the Jaccard index with the Z-score, $Z = (J - \mu_J)/\sigma_J$, where the expectation μ_J and the standard deviation σ_J of the Jaccard index are calculated over 1000 random samples a null model with identical community sizes and random community labels. Clusters from two networks are associated together by repeatedly pairing the two unpaired clusters with the largest z-score. We reported the Z-scores of the best and second best matching community pairs for all community detection algorithms and values of P.

Spectral Clustering Across All Experimental Sessions. We next focused on one method which performed reasonably in the prior analysis (Spectal Clustering into $k = 4$ communities) and applied it to all graphs on all sessions. In this case, to quantify the agreement in community assignments on two graphs with the same nodes, we chose the permutation of assignment labels that maximized the agreement in labels between the two graphs and reported the fraction of labels that agreed. Again, we compared the computed metrics to the same metrics sampled from a null model with identical community sizes and random community labels.

3.4. Modularity of Left/Right Partition

For subsequent analyses, we computed the modularity of the anatomical partition of neurons

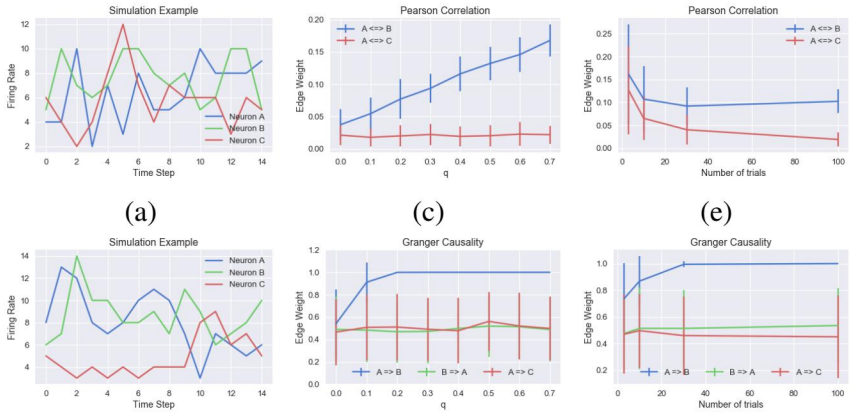

Figure 2. We evaluate the Correlation Network and Causality Network construction method using simulation. Neuron A causally affects neuron B with strength q but B does not causally affect A. All neurons are independent of Neuron C. (a), (b): Sample firing rate time series. (c), (d): Inferred edge weight as neuron interaction strength q increases. (e), (f): Convergence of edge weight inference as the number of trials N increases.

into left and right ALM. We used the following definition of modularity of a partition of an undirected weighted graph with vertices V, adjacency matrix A, partition assignment c_v for each $v \in V$, and node degrees k_v for each $v \in V$:

$$modularity = \frac{1}{2m} \sum_{v,w \in V} (A_{vw} - \frac{k_v k_w}{2m}) I[c_v = c_w]$$

where I is the indicator function.

We focused on applying this analysis to the Granger causality-based graph, as our community detection results suggested that this graph would be most predictive of bilateral perturbation trial structure. We used an unweighted graph, maintaining only the top $P\%$ strongest edges, where P was chosen to be one less than the maximum percentage for which this procedure would yield any nonzero weights. This was done to prune spurious edge weights in the causality graph, of which there are many. Remaining edges were all assigned weight 1. Then undirected weights were assigned for each pair of nodes by adding the edge weights between the nodes in both directions, yielding possible undirected weight values of 0, 1, and 2.

4. Results

4.1. Validating Edge Construction Methods through Simulation

We assessed the ability of our edge construction methods to capture true connectivity patterns in a model of neuron interaction (described in the methods section).

First, we varied the influence of a neuron A on a neuron B by changing q and compute edge weight between neurons A and B and C using the two methods, see Figure 2 (c) & (d). As q increases, the influence of A on B becomes more pronounced. We see both methods capturing this relation. The edge weight between A and B increases, whereas the edge weight between A and C (two disconnected neurons) remains the same. This indicates that both correlatin and Granger causality distinguish connected pairs of neurons from disconnected pairs. Furthermore, we observe that the weight weight for $A \rightarrow B$ increases as q increases, and $B \rightarrow A$ is no more than the baseline value. So Granger Causality indeed captures directional causal relationships and avoids detecting spurious relationships.

We also sought to assess if it is reasonable to expect our algorithm to detect connection be-

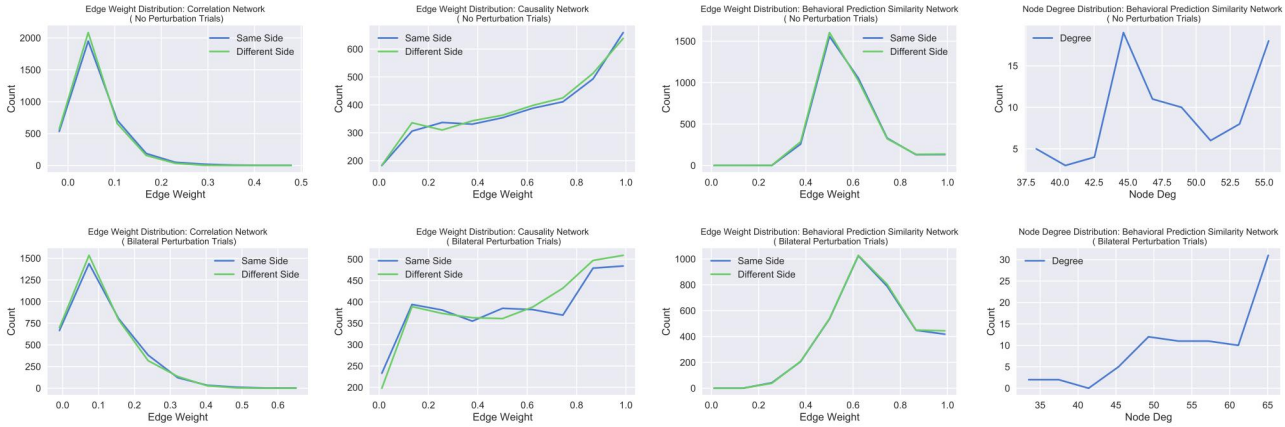

Figure 3. Left three columns: The edge weight distributions, within and across hemispheres, of constructed networks under different perturbation conditions and different graph construction methods. Right column: Node degree distributions for the behavioral prediction similarity networks.

tween neurons given the limited amount of data we have. We varied the number of trials N with q fixed to $q = 0.3$ and computed edge weight between neurons A and B using the two methods, see Figure 2 (e) & (f). As the number of trials increases, the signal to noise ratio increases and both methods distinguish the true interaction of $A \to B$ from the null cases $A \to C$ and $B \to A$. Note that edge weight computed by both methods are relatively accurate at $N = 30$. Our dataset contains more than 30 trials per session (typically on the order of 200 control trials nad 50 bilateral perturbation trials). So under the assumption that our model of neurons is somewhat realistic, we have more than enough trials per session to derive information about the graph.

4.2. Summary Statistics of Inferred Network Structures.

We apply the three methods described in Section 3.2 to data from one of the experimental sessions. Each of the three method generates a weighted graph, either directed (in the case of the Granger causality network) or undirected.

Edge weight distribution. We compare the distriubution of edge weights in control trials and in bilateral perturbation trials (see Figure 3). The correlation networks yield a distribution that appears reasonably Gaussian for both perturbation conditions, and almost all values are relatively low (absolute value less than 0.5), which makes it difficult to assess which correlations are meaningful and detect interesting community structure. The Granger causality networks, on the other hand, yield edge weight distrbutions with peaks at the highest causality strengths, suggesting that many, but not all, neuron pairs do indeed have true (Granger) causal relationships. These statistics are more promising for extracting community structure. The behavioral prediction similarity networks have edge weights mostly greater than 0.5, which makes sense as neurons make correct predictions most of the time. However, the bilateral perturbation data yields a reasonably high number of similarity strengths near 1.0, suggesting that under bilateral perturbation, certain groups of neurons tend to always give the same behavioral prediction, regardless of whether it is correct. These groups are likely to be identified by community detection algorithms. Importantly, the edge weight distribution does not appear to vary significantly when only edges that cross the left/right ALM divide are considered as compared to when only edges within left ALM or within right ALM are considered. This suggests that

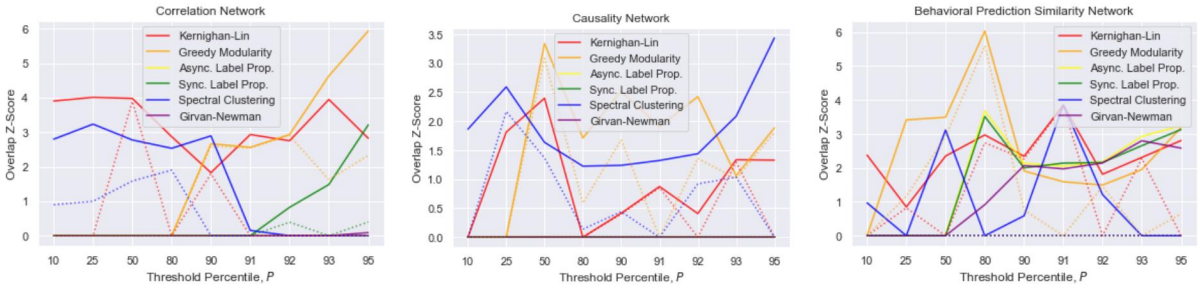

(a) (b) (c)

Figure 4. Z scores, for various community detection algorithms and edge percentile thresholds P, indicating robustness of communities to perturbation as quantified by Jaccard index of top two overlapping communities in the control trial graph and bilateral perturbation trial graph compared to a null model. Solid line indicates Z score for the most robust community, while dashed lines indicate the robustness of the second most robust community.

any left/right modularity in the ALM system is weak, and that the "true" modular structure of these brain regions may involve communities that span both anatomical regions.

Node Degree distribution. We compare the distribution of node degrees in control trials and in bilateral perturbation trials (see Figure 3). The most interesting structure was revealed in the behavioral prediction similarity networks, both of which contained a large number of nodes with very high degree compared to the rest. This suggests that a small number of neurons "drive" the behavioral predictions of many other neurons in the network.

4.3. Community Detection

As described in the Methods section, we applied a panel of community detection algorithms to the control trial and bilateral perturbation trial networks obtained from each of our three edge construction methods (correlation, Granger causality, and behavioral prediction similarity) on an example session. We quantified the extent to which overlap in the most and second most robust (to perturbation) community exceeded that expected in samples from a null model with identical community sizes. The Z-scores of this null model comparison are shown for each P and each method in Figure 4. Many of the methods discover meaningfully robust communities, as indicated by Z-scores that as high as 6. This suggests that these communities are invariant to changes in the network due to perturbation, and therefore, may potentially correspond to biological meaningfully functional modules in the mouse brain.

We also tested the consistency of community assignments by Spectral Clustering with $k = 4$ across all sessions. We found that clusters identified in the correlation network overlapped strongly with clusters in the behavioral prediction similarity network (Figure 5g), indicating that communities coupled neurons tend to give similar predictions. Moreover we found that clusters identified in the causality network were most predictive of clusters in the correlation network for bilateral perturbation trials (Figure 5h), indicating that the *Granger causality network* is best able to predict community structure following perturbation. This may be attributable to the fact that computing granger causality can filter out spurious correlations in the control trial networks.

Visualizations, for an example session, of the various graph structures for control trials and bilateral perturbation trials, with the top two most robust communities indicated, are shown in Figure 5 a-f. The causality network gives the most striking results, as the identified communities clearly persist after perturbation. Notably, the communities span anatomical hemispheres, indi-

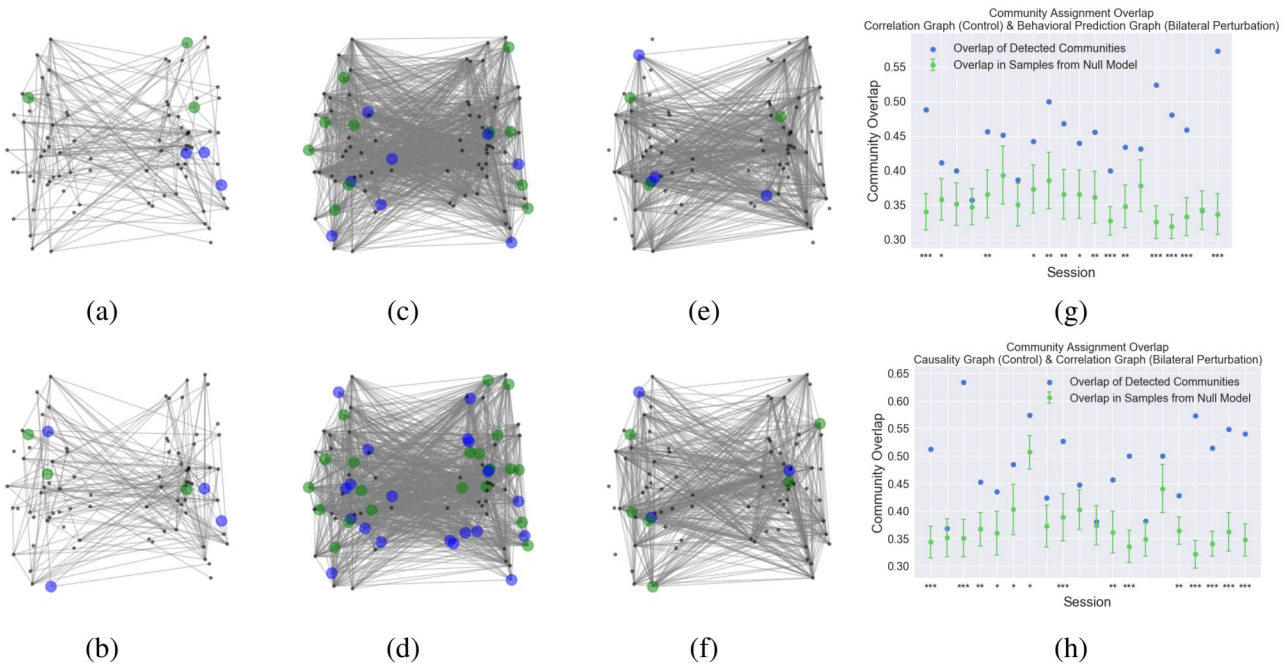

(a) (c) (e) (g)

(b) (d) (f) (h)

Figure 5. (a-f): Visualizations of communities identified by the best-performing method of Figure 4. Green and blue nodes indicate the most and second-most robust communities, respectively. Top row: control trial graphs. Bottom row: bilateral perturbation trial graphs. (a, b): Correlation network. (c, d): Causality network. (e, f): Behavioral prediction similarity network. (g): Quantification of community overlap (using spectral clustering into four communities) across sessions for control trial correlation graph and behavioral prediction similarity graph. (h): Same as (g) but for control trial causality graph and bilateral perturbation trial correlation graph.

cating important network structure beyond that imposed by anatomy.

4.4. Left/Right Modularity Predicts Behavioral and Neural Differences Across Experimental Sessions

In this section, we seek to predict mice behavior using properties of inferred neural connectivity structures. In particular, mice differ in their behavioral responses to the task setup. Some are more accurate at the task than others, and some are more robust to unilateral optogenetic perturbation than others. Even the same mouse will exhibit different behavioral properties across different experimental sessions. We find that the left/right partition modularity of our inferred network structures can predict these cross-mouse and cross-session differences.

Computing Modularity. Using their anatomical location, we classify neurons into two partitions: those belonging to the left ALM and those belonging to the right ALM. This clustering is chosen because unilateral optogenetic perturbation is applied to one side of the two ALM partitions. We compute the modularity of such partition, using both the Granger causality-based network and the behavioral prediction similarity-based network, for all experimental sessions. We measure the correlation between the modularity of a network in a session recording and the corresponding mouse's behavioral performance during that session. See Figure 6.

Metrics. Behavioral accuracy measures the percentage of the trials on which the mouse successfully completes the task. Coding direction recovery quantifies the extent to which the unperturbed hemisphere corrects the firing of the per-

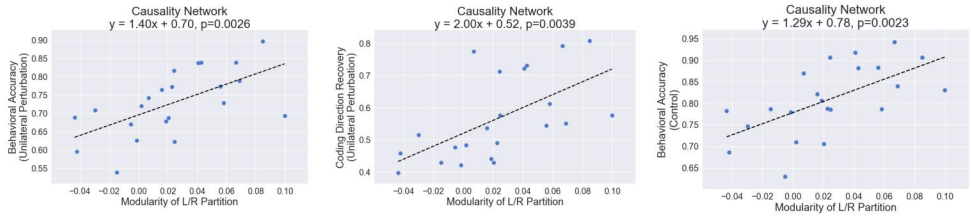

(a) (b) c

Figure 6. Modularity between the left and right ALM area in Granger causality networks correlates with robustness to perturbation and behavioral accuracy, across experimental sessions. (a) Modularity is positively correlated with with behavior accuracy following unilateral perturbation. (b) Higher modularity also correlates with higher recovery rate of neural activity along the coding direction in the perturbed ALM. (c) Modularity also predicts behavioral accuracy on control trials.

turbed hemisphere. It is measured by fraction of recovery to trial-average values for the given trial type. A value of 0 indicates that neuron activity projected onto the coding direction remains at the decision boundary (the mean coding direction activity on all trials). A value of 1 indicates that the firing rates of neurons in the perturbed hemisphere projected onto the coding direction recovers to typical values (e.g. the mean coding direction activity on lick-left trials).

Modularity and Robustness. We found that in the causality graph, modularity of the left/right partition is positively correlated with behavioral accuracy following unilateral perturbation (Figure 6a) with statistical significance. Similarly, higher modularity under the causality network predicts better recovery of coding direction activity (Figure 6b). Our interpretation of these results is as follows. Higher modularity indicates that left and right ALM are less interconnected. Hence, the results suggest that for a mouse to be robust to optogenetic perturbation, it must not have excessively permissive communication between the left and right ALM. Otherwise, perturbation on one side will also corrupt the representation on the other side. Furthermore, we find that the modularity of the network predicts behavioral accuracy even on control trials (Figure 6c). This suggests that even in the absence of experimental perturbation, environmental perturbations and noise in signals from other brain regions add enough uncertainty to the ALM system that modularity is still beneficial in robustly performing the task.

5. Future Work

Future work could extend our work in a number of ways. For instance, we one could explore ways to denoise our edge weights and, when it is necessary to produce unweighted graphs for subsequent analysis, to determine the optimal weight-thresholding procedure more rigorously. One could also seek to validate and characterize the performance of different community detection algorithms on our simulation model of neural interaction. Finally, one could seek to validate the functional significance our identified communities by assessing how successfully a linear dynamical systems model, in which activity evolves independently within each community (potentially allowing for sparse gated interaction with other communities) models the neural activity. In particular, we are interested in the robustness of such a model when applied to perturbation trials. We have already demonstrated the promise of this approach by using the anatomically defined modules, left ALM and right ALM, as test cases, but its application to finer-grained modules is a fascinating direction that could help better understand the functional role of mesoscale structure in premotor cortex.

References

[1] C. M. Aaron Clauset, M. E. J. Newman. Finding community structure in very large networks. *Physical Review E*, 70(066111), 2004.

[2] L. G. Gennaro Cordasco. Community detection via semi-synchronous label propagation algorithms. *The International Workshop on Business Applications of Social Network Analysis*, 2010.

[3] C. W. Granger. Investigating causal relations by econometric models and cross-spectral methods. *Econometrica: Journal of the Econometric Society*, pages 424–438, 1969.

[4] N. Li, K. Daie, K. Svoboda, and S. Druckmann. Robust neuronal dynamics in premotor cortex during motor planning. *Nature*, 532(7600):459, 2016.

[5] Y. Liu, J. Moser, and S. Aviyente. Network community structure detection for directional neural networks inferred from multichannel multisubject eeg data. *IEEE Transactions on Biomedical Engineering*, 61(7):1919–1930, 2014.

[6] S. Nigam, M. Shimono, S. Ito, F.-C. Yeh, N. Timme, M. Myroshnychenko, C. C. Lapish, Z. Tosi, P. Hottowy, W. C. Smith, et al. Rich-club organization in effective connectivity among cortical neurons. *Journal of Neuroscience*, 36(3):670–684, 2016.

[7] G.-G. D. e. a. Pars F. Fluid communities: A competitive and highly scalable community detection algorithm. *Conference on Complex Networks and Their Applications*, 2017.

[8] F. Vecchio, F. Miraglia, F. Piludu, G. Granata, R. Romanello, M. Caulo, V. Onofrj, P. Bramanti, C. Colosimo, and P. M. Rossini. small world architecture in brain connectivity and hippocampal volume in alzheimers disease: a study via graph theory from eeg data. *Brain imaging and behavior*, 11(2):473–485, 2017.

[9] R. Vicente, M. Wibral, M. Lindner, and G. Pipa. Transfer entropya model-free measure of effective connectivity for the neurosciences. *Journal of computational neuroscience*, 30(1):45–67, 2011.

[10] Z. G. Xiaojin Zhu. Learning from labeled and unlabeled data with label propagation. *Technical Report*, 951, 2002.

[11] A. Zalesky, A. Fornito, and E. Bullmore. On the use of correlation as a measure of network connectivity. *Neuroimage*, 60(4):2096–2106, 2012.

6. Appendix: Data Preprocessing Methods

There are 23 experimental sessions, obtained from 7 different mice (some mice participated in more than one session). For each session, a subset of trials and units are selected to (1) ensure that all neurons used are held throughout the specified time window, (2) maximize the number of neurons used, and (3) maximize the number of trials used. Conditions (2) and (3) are at odds given (1), so a heuristic is used to manage the tradeoff.

Spiking data is binned to obtain firing rates using time windows of length 0.4 s, with a stride of 0.1 s (note that adjacent time bins contain substantial overlap). The time window of interest lasts from t = -4 seconds to t = 2 seconds, where t = 0 seconds corresponds to the go cue. The sample period lasts from t = -3 to t = -1.8. Hence t = -1.8 to t = 0 is the delay period and t = -4 to t = -3 is the presample period. Perturbations, when present, last from t = -1.7 to t = -0.9 s. All subsequent analysis is performed using these firing rates. For control trials we consider activity during the entire delay period, and for perturbation trials we consider only post-perturbation activity.

On trials without perturbation, the projections of neural activity in each hemisphere onto each respective coding directions are strongly correlated. Hence, to ensure we identify meaningful correlations in the data, subsequent correlation and Granger causality analysis on control trials is not conducted with raw activity, but rather with the fluctuations of this activity about the conditioned (lick-left or lick-right) trial-average activity. On bilateral perturbation trials no such mean-subtracting is necessary since the perturbation decorrelates the information across hemispheres.